

We are IntechOpen, the world's leading publisher of Open Access books Built by scientists, for scientists

5,800

Open access books available

142,000

International authors and editors

180M

Downloads

Our authors are among the

154

Countries delivered to

TOP 1%

most cited scientists

12.2%

Contributors from top 500 universities



WEB OF SCIENCE™

Selection of our books indexed in the Book Citation Index
in Web of Science™ Core Collection (BKCI)

Interested in publishing with us?
Contact book.department@intechopen.com

Numbers displayed above are based on latest data collected.
For more information visit www.intechopen.com



Chapter

Design and Control of the McKibben Artificial Muscles Actuated Humanoid Manipulator

Daoxiong Gong and Jianjun Yu

Abstract

The McKibben Pneumatic Artificial Muscles (PAMs) are expected to endow the advanced robots with the ability of coexisting and cooperating with humans. However, the application of PAMs is still severely hindered by some critical issues. Focusing on the bionic design issue, this chapter in detail presents the design of a 7-degree-of-freedom (DOF) human-arm-like manipulator. It takes the antagonized PAMs and Bowden cables to mimic the muscle-tendon-ligament structure of human arm by elaborately configuring the DOFs and flexibly deploying the routing of Bowden cables; as a result, the DOFs of the analog shoulder, elbow, and wrist of the robotic arm intersect at a point respectively and the motion of these DOFs is independent from each other for convenience of human-like motion. The model imprecision caused by the strong nonlinearity is universally acknowledged as a main drawback of the PAM systems. Focusing on this issue, this chapter views the model imprecision as an internal disturbance, and presents an approach that observe these disturbances with extended-state-observer (ESO) and compensate them with full-order-sliding-mode-controller (fSMC), *via* experiments validated the human-like motion performance with expected robustness and tracking accuracy. Finally, some variants of PAMs for remedying the drawbacks of the PAM systems are discussed.

Keywords: McKibben artificial muscles, bionic design, anthropomorphic arm, human-like motion, full-order sliding mode control, extended state observer

1. Introduction

Advanced robots, especially the humanoids, are expected to be employed as cooperative robot for coexisting and collaborating with human and interacting with other robots [1] in the human-centered, complex, unstructured, and dynamic daily-living environment, using the tools and equipment designed for human to accomplish some complex tasks or to be adopted as the slave robot to facilitate the tele-manipulation because its human-like configurations is favorable for simplifying the motion mapping as well as improving the efficiency of a homogeneous master-slave system.

Such an ideal humanoid robot must have muscle-like actuators, bionic musculo-skeletal structure (appearance), and human-like motion patterns (behaviors). This chapter will focus and highlight some insights on these topics.

1.1 The McKibben artificial muscles as the bionic actuator

The McKibben Pneumatic Artificial Muscle (PAM) is widely regarded as a promising actuator for robotics and automation [2], and extensive research studies have been conducted to improve its applications in humanoid robot systems. A PAM consists mainly of a rubber bladder with reinforcement knitting nested outside or embedded in it (**Figure 1**). When actuated with a supply of compressed air, it extends in the circumferential direction and contracts in length; as a result, it is able to generate a tensile force high up to hundreds or even thousands Newton and a contraction motion in the longitudinal direction up to 25–37% of its original length. The PAM generates both powerful tensile force and good responsive movement at the start of the contraction and then decreases as it contracts, which behavior is similar to those of a biological muscle.

In a typical situation, a PAM requires a pressure air source and two pneumatic valves, one of which as the inlet valve for filling the air into the PAM, and the other as the outlet valve for exhausting the air out. By controlling the opening of both valves, it is possible to realize the desired contraction/force of the PAM for robot actuation [3].

Because a PAM can only generate a contraction force, people usually adopt a pair of PAMs to mimic the antagonistic configuration (**Figure 2b**) of a human muscle pair actuating a human joint, e.g., the antagonistic muscles pair of the biceps and the triceps brachii efficiently realize the bidirectional motion of the elbow joint, i.e., the



Figure 1. Two kinds of the McKibben artificial muscles (with reinforcement nested outside or embedded in).

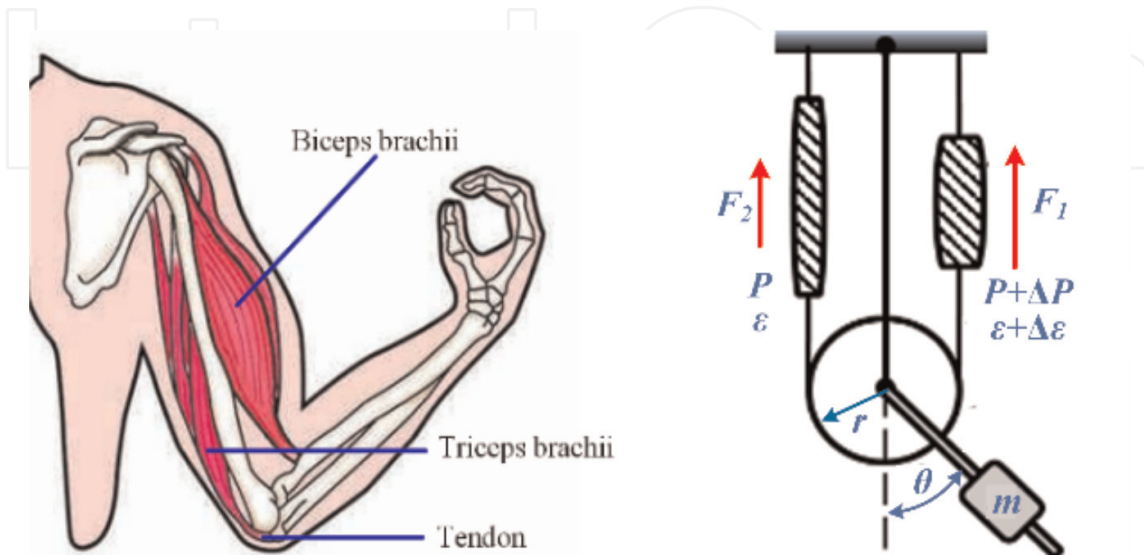


Figure 2. The antagonistic muscles-driven strategy. (a) The human joint; (b) the robotic joint actuated by PAMs via steel wire cables.

elbow flexes when the biceps contracts and the triceps relax, and the elbow straightens when the biceps relaxes and the triceps contracts (**Figure 2a**). By combining the PAMs and the steel wire rope as an artificial muscle-tendon structure and attaching the ropes on the pulley circumference of the robotic joint, people can conveniently keep the direction of contraction/relaxation of the PAMs unchanged, avoid the misalignment of the PAMs, and keep the linear relationship between the contraction/relaxation length of PAMs to the rotation angle of the robotic joint:

$$\varepsilon = r\vartheta \quad (1)$$

where ε is the length of contraction/relaxation of the antagonistic PAM pair, r the pulley radius and ϑ the rotation angle of the pulley in radian, and it should cover the rotary scope of the concerned joint.

PAMs possess compelling properties in various aspects [4], including the inherent compliance, the actuating characteristics similar to those of the human muscle, high power-to-mass and power-to-volume ratio, flexibility of deployment, low cost, etc. Therefore, researchers have conducted vast studies in recent years and have gotten a lot of progress in the robot application study of PAMs.

1.2 The bionic design of humanoid robots actuated by PAMs

PAMs are widely regarded as an ideal actuator for cooperative robots because its actuating properties are similar to those of the human muscles and its inherent compliance stems from the mediator of compressible air. Therefore, people are prone to realize the human-like dexterous and compliant manipulation by mimicking both the organization and the actuating characteristics of the human muscles with PAMs.

Researchers studied the structure of human arm/hand and mimicking the configuration features in the robot designation to realize the human-like dexterity and have invented many anthropomorphic musculoskeletal robot systems. The famous FESTO Airic's arm [5] and SHADOW Hand [6] are two examples of the bionic musculoskeletal robot arm/hand, respectively. The FESTO Airic's arm imitates the structure of human arm with highly similarity. It consists of the ulna, the radius, the metacarpal and phalanges, a shoulder ball joint, and the scapular structure actuated by 30 FESTO Fluidic muscles to imitate the arrangement of the muscles of the human arm (**Figure 3**



Figure 3.
The bionic musculoskeletal robots of the FESTO Airic's arm and the SHADOW hand [5, 6].

left). The Shadow Hand is designed to replicate the functionality, dimensions, and range of motion of the human hand (**Figure 3** right). With 20 DOFs actuated by PAMs as well as touch sensors mounted on the fingertips, the Hand as a slave robot end-effector is able to precisely mimic the master operator's movements to complete complex teleoperation tasks.

In order to achieve highly human-like dexterity, researchers even try to replicate the manipulation dexterity of human hand in the robotic system via highly biomimetic design. For example, Nanayakkara et al. reviewed the unique musculoskeletal structure of the human hand for inspiring the design of robotic hand to improve its dexterous grasping and manipulating capabilities [7]; Xu et al. designed a biomimetic robotic hand that closely mimics the human hand with artificial joint capsules, crocheted ligaments and tendons, laser-cut extensor hood, and elastic pulley mechanisms [8]; Faudzi et al. designed an index finger of human-like robotics hand that closely replicates the human finger in terms of bones, ligaments, thin McKibben PAMs, extensor mechanism, tendon, and pulley system [9]; Tasi et al. designed an anatomically correct, biomechatronic hand that emphasizes the anatomical consistency with the human hand and implements every functionally significant bone, ligament, finger-actuating intrinsic and extrinsic muscles, tendinous network, and pulley system to realize the same synergistic movements of the human hand [10]. Ikemoto et al. designed a musculoskeletal robot arm driven by PAMs to mimic the structure of the human shoulder complex and try to assure a wide range of movements and the joint's stability at the same time [11].

However, a robotic arm with highly similarity in construction to the human arm will certainly lead to a very complex and elaborated mechanical structure, which may pose a challenge to both the manufacture and the motion control of the system. Therefore, people should emphasize more similarity to human arm in functionality than in construction when they conceive the design scheme of the robotic arm, especially they should pay attention to the scheme that is able to eliminate the coupling effect among DOFs to facilitate the human-like motion control of the robotic arm.

Some of the human arm joints can be viewed as a spherical joint. A spherical joint actuated by muscle groups may lead to strong coupling between the tensile forces of the muscles, which will make the motion control of the joint difficult. People usually decompose the motion of a spherical joint into two or three orthogonal rotation axes with every rotation axis actuated by a pair of antagonistic muscles. However, if the robotic orthogonal rotation axes of a counterpart of the human joint (e.g., shoulder) are not intersecting at one point, the motion of different DOFs may become coupling and lead to unnatural or not human-like movement of the robotic arm [12, 13].

This is a critical issue need to be solved for promoting the PAM application in the humanoid robotic systems. This chapter will illustrate a solution to this issue via an example of robotic manipulator system.

1.3 The strong nonlinearity and modeling/control problem of PAMs

It is generally agreed that it is very difficult to model PAM precisely, and the model imprecision, which caused by both nonlinearities (including hysteresis effects) and the uncertainty of parameters, will severely impede the control performance of the PAM system.

Extensive studies have been conducted by researchers to improve the control performance of PAM systems.

As a widely regarded powerful robust nonlinear control scheme, the Sliding Mode Control (SMC) and its many varieties, e.g., the SMC [14], the second-order SMC [15], the hybrid of SMC and adaptive fuzzy Cerebellar Model Articulation Controller [16], the Nonsingular Terminal SMC [17], the fuzzy terminal SMC [18], etc., have been adopted to control the PAM systems and have shown a vast potential for the application of SMC in the PAM system. Besides the miscellaneous modeling and control methods, a lot of intelligent modeling methods and control algorithms, e.g., the modeling method based on machine learning [19] or artificial neural networks [20], as well as the control algorithms based on learning vector quantization neural network [21], fuzzy control [22], and nonparametric control algorithms [23], have been studied.

Though these studies have demonstrated some exciting results, the model inaccuracy problem of PAM device and the nonlinearity-caused control difficulty of the PAM system still need further studies. This chapter will present an effective solution to this problem via a case study.

1.4 The human-like motion control of the PAM systems

Human-like motions are critical for a robot to coexist and collaborate with human, as well as interact with other robots [1], in the human-centered, complex, unstructured, and dynamic daily-living environment. The anthropomorphic features of the robot and the human trust motion pattern of the robot have been experimentally validated to be very important for performing human-robot collaboration tasks [24]. A human cooperators will feel comfortable and friendly if the robot exhibits the human-like behaviors, which are predictable and understandable for the human partner involved in the collaboration [25]. Otherwise, an unexpected speed variation of a robotic arm will increase the “surprise” subjective rate, cause the mental strain of human cooperators, and reduce the efficiency of human-robot cooperation [26]. Therefore, it is important to make the robot’s motion patterns natural, understandable, and predictable to the human cooperators for effective human-robot collaboration [27].

Studies in physiology, anatomy, biomechanics, and neuroscience have revealed that human motion has its own special characteristics [28]. The motion of human arm in the free space is assured satisfying the minimum jerk model, i.e., the motion of the human arm conforms to the Logistic Equation and shows a bell-shaped velocity profile [29].

To realize the expected human-like motion on a robotic manipulator actuated by PAMs is a tracking control problem of the nonlinear robotic system. This chapter will concern and present a feasible solution to it.

2. Bionic design of humanoid manipulator

As mentioned above, a highly biomimetic design may lead to a very elaborated mechanical structure and pose a challenge to manufacture and motion control of the system. Especially, a spherical joint actuated by muscle groups may cause strong coupling between the tensile forces of the muscles and make the motion control difficult. To decompose the motion of a spherical joint into two or three orthogonal rotation axes is an option, but if these robotic orthogonal rotation axes of a spherical joint cannot intersect at one point, the motion of the robotic arm may become unnatural or not human-like and consequently degrade the robot system.

A design scheme of a human-arm-like manipulator actuated by antagonized PAM pairs that nicely solved this problem is presented in the following sections.

The following measures are taken to endow the humanoid robotic manipulator the ability of reproducing the motion of human arm/hand and easy cooperating with human:

1. The DOF configurations of the robotic arm are similar to those of human arm;
2. The mechanical structure should be as simple as possible for easy fabrication, assembling, and maintenance;
3. The motion of every DOF is independent from each other for reducing the effect of coupling and easy control.

2.1 The 7-DOF human-arm-like manipulator actuated by antagonized PAMs

2.1.1 The kinematic model of the robotic arm

The designed robotic arm possesses a shoulder joint with three DOFs (flexion/extension, abduction/adduction and internal/external rotation of the upper arm), and an elbow joint with two DOFs (flexion/extension and pronation/supination of the forearm) and a wrist joint with two DOFs (flexion/extension, abduction/adduction of the hand). The same DOF configuration, the same joint motion range (**Table 1**), as well as the same proportion of limb length of the Master Motor Map (MMM) kinematic model [30] are taken in the robot arm's design scheme [31]. As shown in **Figure 4**, 7 joints of the robotic arm are independently actuated by a pair of antagonistic PAMs (the circles and arrows in different color indicate the joints actuated by different PAMs as illustrated in **Figures 6–8**). This DOF configuration of the robotic arm makes sure that the three joints of its analog shoulder, the two joints of its analog elbow, as well as the two joints of its analog wrist intersect at a common point, respectively. These structural features make the robotic arm kinematically homogeneous to the human arm; as a result, the robot arm is able to reproduce the motion of human arm with the human-like flexibility, e.g., to recover from errors, to avoid singularity, and to perform obstacle avoidance. Furthermore, this DOF configuration as well as the mechanical structure of the joints of the robotic arm as described below will make the motion of the adjacent joints decoupled and consequently convenient for the motion control of the robotic arm.

2.1.2 The configuration of PAMs and cables in the robotic arm

Generally, an anthropomorphic robotic arm means that a very complex and elaborated mechanical structure is needed, and the whole system may become very difficult

Joint	DOF	X-limits	Z-limits	Y-limits
Shoulder	3	$[-120^\circ, 90^\circ]$	$[-90^\circ, 30^\circ]$	$[-60^\circ, 60^\circ]$
Elbow	2	$[0^\circ, 135^\circ]$	—	$[-90^\circ, 90^\circ]$
Wrist	2	$[-30^\circ, 30^\circ]$	$[-60^\circ, 60^\circ]$	—

Table 1.
The range of motion of each DOF.

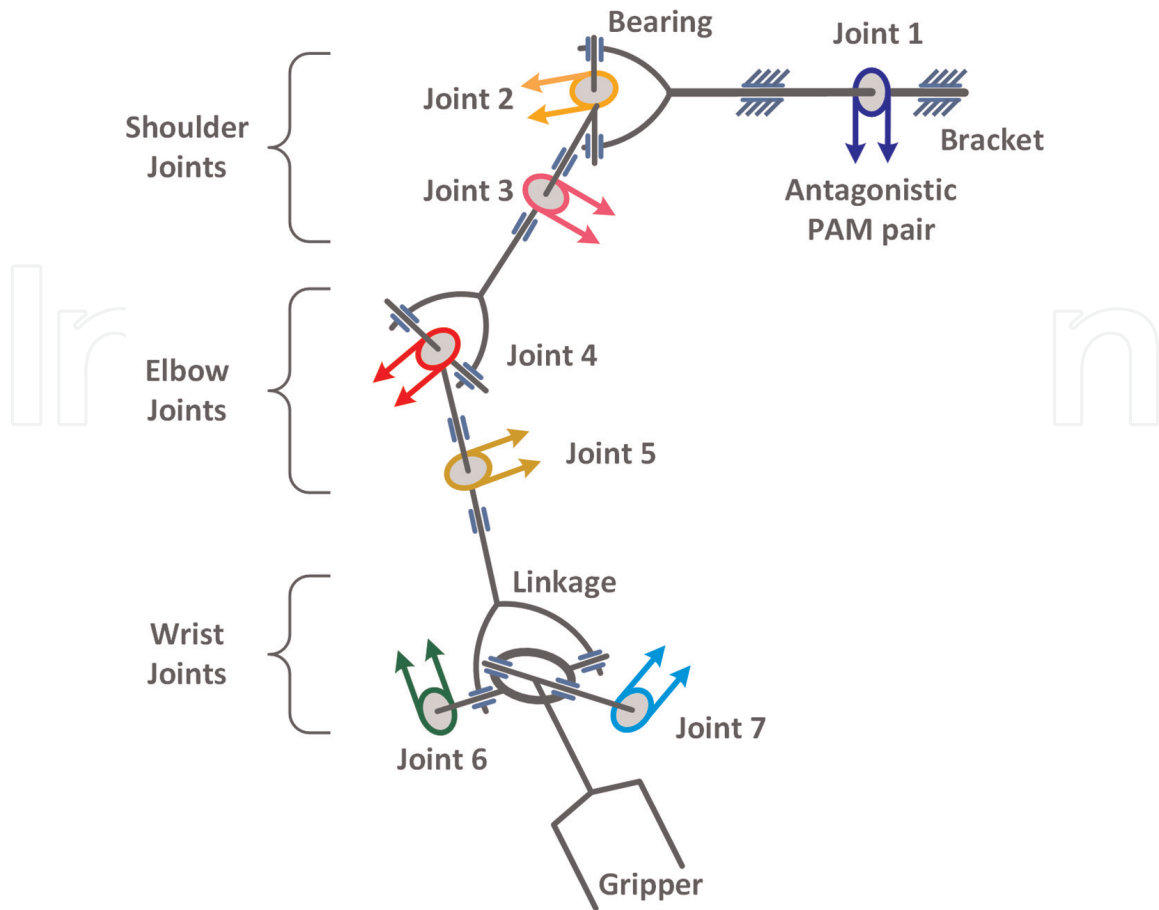


Figure 4.
The DOF configuration and the joint actuating scheme of the humanoid arm.

to control. In order to facilitate the actuation/control of the humanoid arm, Bowden cables are adopted to decouple the tensile forces of the different antagonistic PAM pairs.

The Bowden cable consists of an outer sheath and an inner tendon, the inner tendon (with diameter of 1.5 mm) is used for actuation transmission of every DOF, and the outer sheath is used for guiding the motion of the inner tendon in a curved path that gets over the moving adjacent DOF. As a result, the motion of the concerned DOF will not be disturbed by the motion of the other DOFs. The Bowden cable scheme has many advantages, e.g., lightweight, space saving, and especially the flexible layout of PAMs on the robot without suffering from misalignments, which make it a suitable solution for the PAMs actuation transmission of the robotic system.

The designed humanoid robotic arm is composed of a torso, an upper arm (386 mm in length), a forearm (342 mm in length), and a hand as shown in **Figure 5**. The pressure air source is placed under the table, and the valves and air pipelines are placed on the shelf behind the robot. Both of the upper arm and the forearm have a bar placed on the center to serve as the skeletons, and four PAMs are installed evenly around the bar as the muscles. The torso is an aluminum frame used to support the robotic arm, and six PAMs are installed on the torso as the muscles to actuate the shoulder joint. Bowden cables are adopted as the tendons to transmit the actuation force to the DOFs of the joint of the shoulder, the elbow, and the wrist, respectively.

Though the shoulder complex usually is considered as the most complicated part of the human body as well as with the greatest range of motion than any other joint in the body, the motion of the three DOFs of the robotic shoulder joint can be decoupled via the elaborative arrangement of Bowden wires.

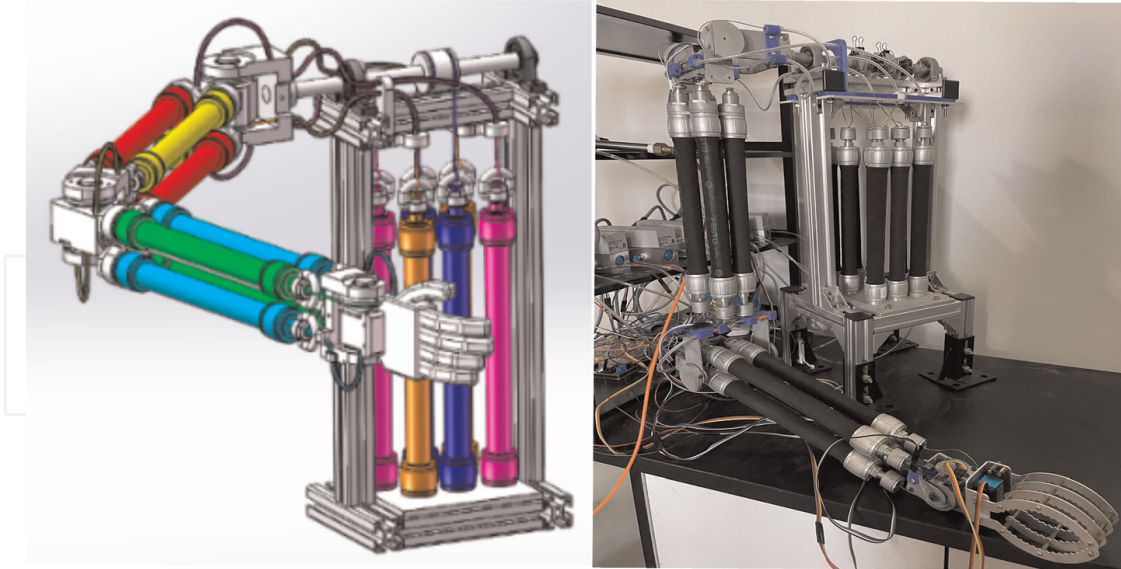


Figure 5.
The structure and the physical device of the 7-DOF humanoid arm actuated by PAMs [31].

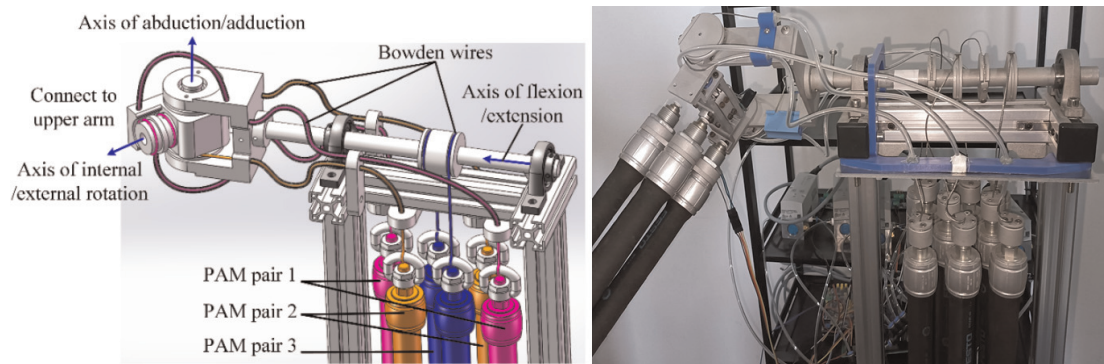


Figure 6.
The structure and the physical device of the shoulder joint [31].

As shown in **Figure 6**, the robotic shoulder consists of three DOFs, the first one for the flexion/extension of the upper arm (actuated by PAMs in blue), and the second one for the abduction/adduction of the upper arm (actuated by PAMs in orange), and the third one for the internal/external rotation of the upper arm (actuated by PAMs in magenta). One end of these PAMs is fixed on the framework of the torso and another end is attached to the corresponding axis of DOF via Bowden cables. The outer sheath in orange bypasses the DOF of flexion/extension and attached on the fixed part of the DOF of adduction/abduction, while the inner tendon is attached on the rotation part of the DOF of adduction/abduction. Also, the outer sheath in magenta bypasses the DOFs of both flexion/extension and adduction/abduction and attached on the fixed part of the DOF of internal/external rotation, while the inner tendon is attached on the rotation part of the DOF of internal/external rotation. Consequently, the motions of the three DOFs of the shoulder joint are independent from each other, and the control algorithm of these DOFs can be separately designed without needing to consider their coupling (or interaction) effect.

As shown in **Figure 7**, the elbow joint consists of two DOFs, one for the flexion/extension of the forearm (actuated by PAMs in red), and another for the pronation/supination of the forearm (actuated by PAMs in yellow). One end of these PAMs is

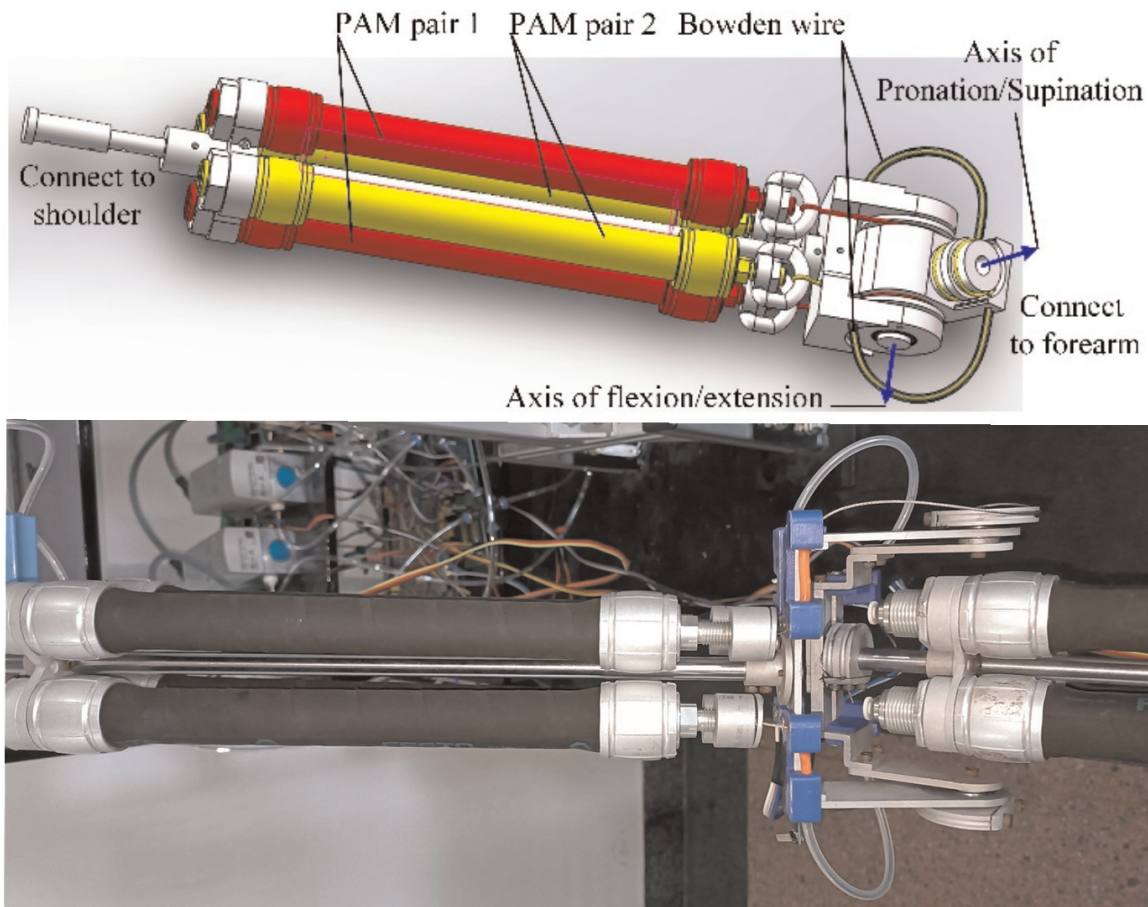


Figure 7.
The structure and the physical device of the elbow joint [31].

fixed on the framework of the upper arm and another end is attached to the corresponding axis of DOF via Bowden cables. The outer sheath in yellow bypasses the DOF of flexion/extension and attached on the fixed part of the DOF of pronation/supination, while the inner tendon is attached on the rotation part of the DOF of pronation/supination. Consequently, the motions of flexion/extension and pronation/supination of the elbow joint are independent from each other, and the control algorithm for these two DOFs can be separately designed without needing to consider their coupling (or interaction) effect.

As shown in **Figure 8**, the wrist joint consists of two DOFs, one for the flexion/extension of the hand (actuated by PAMs in green) and another for the abduction/adduction of the hand (actuated by PAMs in blue). One end of these PAMs is fixed on the framework of the forearm and another end is attached to the corresponding axis of DOF via Bowden cables. The outer sheath in blue bypasses the DOF of flexion/extension and attached on the fixed part of the DOF of abduction/adduction, while the inner tendon is attached on the rotation part of the DOF of abduction/adduction. Consequently, the motions of flexion/extension and abduction/adduction are independent from each other, and the control algorithm for these two DOFs can be separately designed without needing to consider their coupling (or interaction) effect.

Because the kinematic configuration of the designed robotic arm is the same as that of the MMM human arm reference model, the robotic arm is able to reproduce the motion of human arm. Due to the uniqueness of the joint design and Bowden cable arrangement, each DOF of the designed humanoid robotic arm is independently actuated by a pair of antagonistic muscles, and the motion of each DOF is decoupled

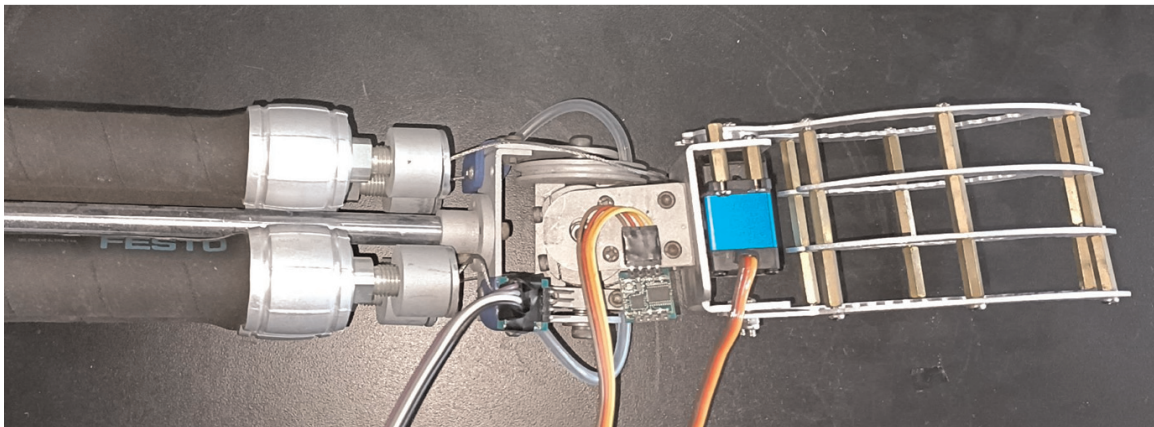
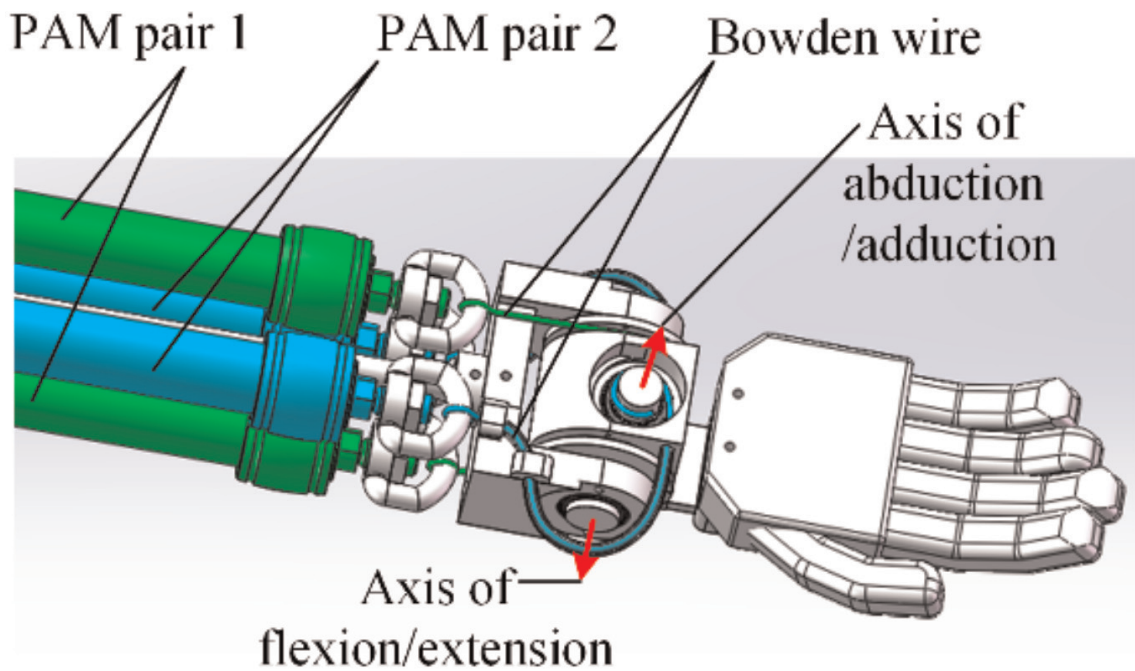


Figure 8.
The structure and the physical device of the wrist joint [31].

from each other. As a result, the mechanical structure of the robotic arm is simple, easy to be assembled, maintained, and controlled.

2.2 The design highlights for the anthropomorphic robotic hand

As shown in **Figure 8**, a gripper is attached on the robotic wrist. However, in order to endow the robotic systems the capability of human-like dexterous manipulation and easily cooperating with human, an anthropomorphic hand that mimics the functions of the human hand is essential, and the following factors should be taken into consideration in the design scheme of such a robotic hand [32]:

1. The robotic hand should be kinematically similar to the human hand (e.g., the MMM model) so that it is able to perform the same motions of the human hand. The DOF configuration of the human hand is very important for its delicate manipulations. For example, the abduction/adduction motion of the metacarpophalangeal (MCP) joint of the fingers (especially the thumb) for anthropomorphic grasping and the transverse metacarpal arch motion of the palms for scooping things. These DOF

configurations as well as their corresponding motion ranges should be carefully considered and realized in the robotic hand design.

2. The bionic design should focus on the similarity to human hand in functionality instead of construction, so that the mechanical structure is simple for easy fabrication, assembly, and maintenance and control. In order to do this, the aforementioned design scheme of the robotic arm can be used for reference of the design of the robotic hand, especially the DOF configurations as well as the routing of the Bowden cables for decoupling the motions of the orthogonal DOFs of the MCP joints. PAMs and Bowden cables are taken as analog of muscle-tendon-ligament structure to actuate each DOF of the robotic hand with a pair of antagonistic PAMs and Bowden cables for avoiding the motion coupling of adjacent joints. Though a human hand has both intrinsic and extrinsic muscles, all the PAMs should be arranged as extrinsic muscles and placed far away from the hand for not hindering the manipulation of the robotic hand because of the volume of the PAMs.

3. Air bladders can be attached at the robotic hand palm and finger segments as analog of the soft muscle pads and skin of human hand for mimicking the haptic sensing of the skins. Muscles and skin on the human hand bring it the capabilities of soft touch and tactile feedback, which is very important for dexterous robotic hand operating an object or interacting with human appropriately via motion/force control. Pneumatic tactile sensors based on air bladder possess some noticeable advantages for human-robot interaction application. The air bladder-based pneumatic tactile sensor is able to sense the lumping force acted on the chamber by measuring the pneumatic pressure change in the air bladder [33], and the air bladder itself is flexible for bending, stretching, and adapting to different mechanical structure on the robot. Regular textures can be designed on the bladders of the fingertip to mimic the fingerprint for enhancing the roughness sensing via the vibration signals generated when the fingertip slides on a rough surface. With the air bladder-based pneumatic tactile sensors as the pad of the fingers, the robotic hand is able to physically interact with humans and the environment via the “human-like compliant touch.” Because of the inherent compliance of the mediator of compressible air in the bladder, the robotic hand is able to yield to unexpected impact when it collides with obstacles (environment or human) and then accordingly take measures to guarantee the safety of the robot system itself, the human, and the environment. With the air bladder-based pneumatic tactile sensors, the robotic hand may also explore the environment in a manner of “action for perception” [34] to obtain the information of the roughness of the object surface, the softness/stiffness of the object, and the slippage of an object grasped in the hand. Furthermore, the robotic hand is able to achieve a stable grasp as well as other manipulation tasks via force control based on the tactile sensing information.

2.3 Summary

Highly biomimetic design that mimics the musculoskeletal structure of human arm will inevitably lead to high structural complexity and control difficulty of the robotic system. Especially the spherical joint may lead to the motion of its decomposed orthogonal DOFs coupling, or lead to the movement of the robotic arm unnatural or

not human-like because the rotation axes of these DOFs do not intersect at one point. Via the detailed bionic design of a 7 DOF human-arm-like manipulator, this section illustrated the DOFs' elaborate configuration and the Bowden cables' flexible routing scheme that successfully make the DOFs of a spherical joint intersected at a point and the motion of these DOFs independent from each other, so that the motion control and human-like dexterous manipulation can be conveniently realized on the PAMs actuated robotic system.

This example also exhibited the advantage of flexible layout of the PAMs in the actuation of robotic systems. If motors instead of PAMs are taken as the actuators of the robotic arm, it will be very difficult to make the DOFs of a spherical joint to intersect at a point, and the robotic arm will be offset and bulky because of the volume issue of the motors and reduction gears, which must be coaxially mounted on the axis of the DOF. While the PAMs can be placed far away from its actuated DOF, therefore the robotic manipulator actuated by PAMs may be small in size and light in weight for dexterous and convenient manipulations.

3. Human-like motion control for a PAMs-actuated robotic joint

As mentioned above, it is universally acknowledged that the difficulty of controlling a PAM system lies in the strong nonlinear characteristics of PAMs, and advanced control algorithms are urgently needed for making the best use of the advantages and bypassing the disadvantages of PAMs. In order to solve this problem, an fSMC-ESO algorithm [35] that combines the Extended State Observer (ESO) and the full-order Sliding Mode Controller (fSMC) for a robotic joint actuated by a pair of antagonistic PAMs is presented in the following sections. In this fSMC-ESO algorithm, the fSMC is adopted to eliminate the chatter and guaranteeing the finite-time convergence and the ESO to observe both the total disturbance and the states of the robot system. Experiments validate that the fSMC-ESO algorithm can efficiently inhibit the disturbance and compensate both the nonlinearity and the modeling inaccuracy to achieve good control performance of the PAM system.

3.1 The human-like motion pattern

According to the study of Flash et al. [36], assuming the movement to start and end with zero velocity and acceleration, the free motion trajectory of the human hand satisfies the minimum jerk model and conforms the Logistic Equation as follows:

$$\begin{cases} x(t) = x_0 + (x_0 - x_f)(-10\tau^3 + 15\tau^4 - 6\tau^5) \\ y(t) = y_0 + (y_0 - y_f)(-10\tau^3 + 15\tau^4 - 6\tau^5) \end{cases} \quad (2)$$

where $\tau = t/t_f$ is time variable, (x_0, y_0) , (x_f, y_f) are the position of the human hand at the initial time ($t = 0$) and the final time ($t = t_f$), and -10 , $+15$, -6 are constant coefficients, respectively.

Consequently, for the motion of a robotic joint's, the desired value of the joint angle x_d , the angular velocity \dot{x}_d , and the angular acceleration \ddot{x}_d will change over time according to the following human-like motion equations:

$$\begin{cases} x_d = x_f(10\tau^3 - 15\tau^4 + 6\tau^5) \\ \dot{x}_d = x_f(30\tau^2 - 60\tau^3 + 30\tau^4)/t_f \\ \ddot{x}_d = x_f(60\tau - 180\tau^2 + 120\tau^3)/t_f^2 \end{cases} \quad (3)$$

where x_f is the maximum rotation angle of the joint. The initial value of joint angle, the initial/final angular velocity, and the initial/final angular acceleration are zero.

3.2 Mathematical model of a robotic joint actuated by antagonistic PAMs

As illustrated in **Figures 4–8**, every joint of the designed robotic arm is independently actuated by a pair of antagonistic PAMs because the motions of adjacent joints are decoupled by the arrangement of Bowden cables. Therefore, this chapter only presents the human-like motion control scheme for a single joint system as shown in **Figure 9**. This experiment platform is a simplification of the robotic arm system of **Figure 5**. With only a single joint actuated by a pair of antagonistic PAMs, it simulates the weight lifting motion via the upward flexion of the elbow joint or the abduction of the shoulder with the elbow extended. The following control scheme for single joint can be easily promoted to the multiple joints of the robotic arm since the motions of its joints are independent from each other.

For the bionic robotic joint actuated by antagonistic PAMs of **Figure 9**, its mathematical model based on Yu's PAM model [37] is:

$$F(\varepsilon, p) = k_1(p) - k_2(p)\varepsilon + k_3(p) \exp(-\mu\varepsilon) \quad (4)$$

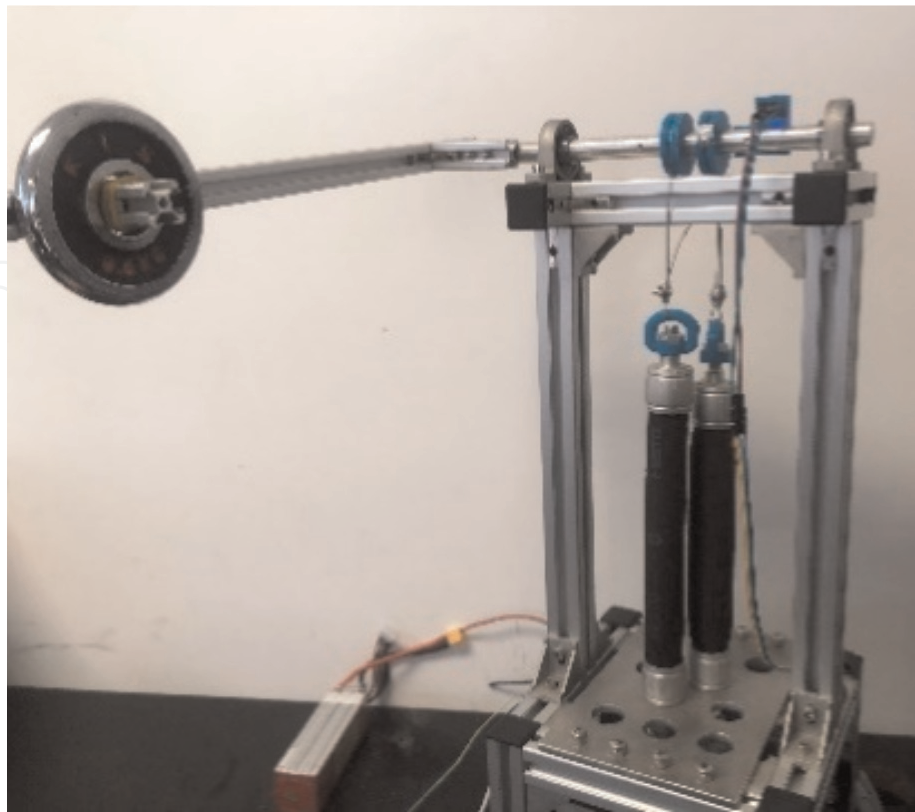


Figure 9.
 The experimental platform of the bionic robotic joint actuated by antagonistic PAM pair.

where F is the output force of PAM; $\varepsilon = (L_0 - L)/L_0$ is the contraction rate of PAM; L_0, L are the original length and the actual length of PAM, respectively; p is the inner pressure of pneumatic muscles; $k_i(p) = k_{i1}p + k_{i2}$, ($i = 1, 2$) are pending coefficients depended on p , k_{i1} and k_{i2} are fitting coefficients that are different in the inflation and the deflation processes; μ is the nonlinear attenuation coefficient of ε . Yu's PAM model consists of two parts, i.e., the model of the inflation process and those of the deflation process, and there is an obvious hysteresis between the inflation and deflation processes. In this study, only the inflation part of the Yu's model is adopted to modeling the robotic joint for convenient of computation, and the compensation of the model inaccuracy of the robotic joint (including those caused by the incompleteness of the PAM model) relies on the control algorithm.

Rewritten Eq. (4) as:

$$F(\varepsilon, p) = (k_{11}p + k_{12}) - (k_{21}p + k_{22})\varepsilon + (k_{31}p + k_{32}) \exp(-\mu\varepsilon) = g(\varepsilon)p + h(\varepsilon) \quad (5)$$

where

$$\begin{aligned} g(\varepsilon) &= k_{11} - k_{21}\varepsilon + k_{31} \exp(-\mu\varepsilon) \\ h(\varepsilon) &= k_{12} - k_{22}\varepsilon + k_{32} \exp(-\mu\varepsilon) \end{aligned} \quad (6)$$

The dynamic equation of the bionic robotic joint is as follows:

$$J\ddot{\theta} + f_b\dot{\theta} = (F_1 - F_2)r - mgl \sin(\theta) + d \quad (7)$$

where $J = m_{pulley}r^2/2 + ml^2$ is the equivalent moment of inertia of the bionic joint, m_{pulley} is the mass of the pulley; m is the mass of the load; r is the radius of the pulley; l is the equivalent length of the connecting rod; θ is the rotation angle of the joint; $f_b\dot{\theta}$ is the damping term of the joint where the f_b is damping coefficient; F_1 and F_2 are the forces exerted by the antagonistic PAMs; d are the (external and internal) disturbances caused by the system parameter uncertainties.

Substituting the forces (5) of the antagonistic PAMs into (7):

$$J\ddot{\theta} + f_b\dot{\theta} = (g(\varepsilon_1)p_1 - g(\varepsilon_2)p_2 + h(\varepsilon_1) - h(\varepsilon_2))r - mgl \sin(\theta) + d \quad (8)$$

The antagonistic forces exerted by each PAM of the antagonistic pair should remain greater than 0 at all time, i.e., $F_1(t) > 0$, $F_2(t) > 0$, for $t \geq 0$. Therefore, the actual lengths of the PAMs are:

$$\begin{cases} L_1 = L_{1init} - r\theta \\ L_2 = L_{2init} - r\theta \end{cases} \quad (9)$$

where L_{1init}, L_{2init} are the initial lengths of the antagonistic PAMs when the rotation angle of the joint is $\theta = 0$.

Select the state variables as $x_1 = \theta$ and $x_2 = \dot{\theta}$, then the state equations of the studied joint are:

$$\begin{cases} \dot{x}_1 = x_2 \\ \dot{x}_2 = \frac{(h(\varepsilon_1) - h(\varepsilon_2))r - mgl \sin(x_1) - f_b x_2}{J} + \frac{(g(\varepsilon_1)p_1 - g(\varepsilon_2)p_2)r}{J} + \frac{d}{J} \end{cases} \quad (10)$$

Formulating $f(x) = [(h(\varepsilon_1) - h(\varepsilon_2))r - mgl \sin(x_1) - f_b x_2]/J$, $b = r/J$, $d_j = d/J$, and $u = g(\varepsilon_1)p_1 - g(\varepsilon_2)p_2$ as the control input, then,

$$\begin{cases} \dot{x}_1 = x_2 \\ \dot{x}_2 = f(x) + bu + d_j \end{cases} \quad (11)$$

This is a second-order nonlinear system with its control inputs u decided by the inner pressures of the antagonistic pair of PAMs, i.e., p_1 and p_2 , which can be controlled to achieve the expected human-like motion of the studied robotic joint.

3.3 The full-order sliding mode control with extended state observer

The fSMC sliding surface is adopted as follows [38]:

$$s = \ddot{e} + c_2 \text{sign}(\dot{e})|\dot{e}|^{\alpha_2} + c_1 \text{sign}(e)|e|^{\alpha_1} \quad (12)$$

where constants $c_1 = 16$, $c_2 = 6$, $\alpha_1 = 5/8$, $\alpha_2 = 5/11$, and $\dot{e} = \dot{x}_d - \dot{x}_1$, $\ddot{e} = \ddot{x}_d - \ddot{x}_1$ are the first and second derivatives of e , $e = x_d - x_1$ is the tracking error of the joint, x_d , x_1 are the expected and the actual value of the joint angle, respectively.

The control input u is [38]:

$$u = -b^{-1}(u_{eq} + u_n) \quad (13)$$

where

$$u_{eq} = -\ddot{x}_d + f(x) - c_2 \text{sign}(\dot{e})|\dot{e}|^{\alpha_2} - c_1 \text{sign}(e)|e|^{\alpha_1} \quad (14)$$

$$\dot{u}_n + Tu_n = -\eta \text{sign}(s) \quad (15)$$

The Eq. (15) can serve as a low-pass filter to inhibit the high-frequency disturbance and to enhance the robustness of the system. Where $T = 0.01\text{Hz}$ is the bandwidth of the low-pass filter, and $\eta = 5$ is the control gain term.

Based on Eq. (11), an extended state $x_3 = f(x) + d_j$ is defined as the total disturbance (including both the external and the internal disturbances) estimated by the ESO, and consequently, a new model of the studied robotic joint system can be described with the new set of state variables:

$$\begin{cases} \dot{x}_1 = x_2 \\ \dot{x}_2 = x_3 + bu \\ \dot{x}_3 = \dot{f}(x) + \dot{d}_j \\ y = x_1 \end{cases} \quad (16)$$

Define z_1 , z_2 and z_3 as the estimated value of the state variable x_1 , x_2 and x_3 , respectively, then the model of the tracking control system is:

$$\begin{cases} e_1 = z_1 - y \\ \dot{z}_1 = z_2 - \beta_{01}e_1 \\ \dot{z}_2 = z_3 - \beta_{02}e_1 + bu \\ \dot{z}_3 = -\beta_{03}e_1 \end{cases} \quad (17)$$

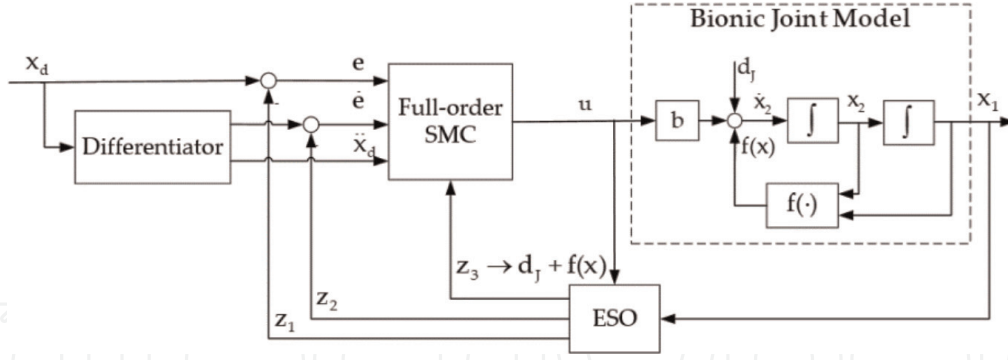


Figure 10.
Block diagram of the fSMC-ESO tracking control system.

where

$$[\beta_{01} \ \beta_{02} \ \beta_{03}]^T = [3\omega \ 3\omega^2 \ \omega^3]^T \quad (18)$$

are positive constants and $\omega = 150\text{rad/s}$ according to reference [39].

As described above, the fSMC-ESO scheme views the model inaccuracy as a kind of internal disturbances and combines ESO and fSMC for achieving the human-like motion control of the robotic joint actuated by a pair of antagonistic PAMs.

The block diagram of the studied tracking control system is shown in **Figure 10**. In **Figure 10**, x_d and \ddot{x}_d are the desired joint angle and the angular acceleration, which are computed with Eq. (3), of the human-like motion of the concerned robotic joint, respectively; e and \dot{e} are the tracking error and its first derivative of the joint as explained in Eq. (12); the full-order SMC block consists of the Eqs. (12)–(15), which is chattering free and especially suiting for higher-order nonlinear systems with both uncertainty parameters and external disturbance [38]; the Bionic Joint Model block is the mathematic model of the concerned robotic joint as described in Eq. (16); and the ESO block is the extended state observer of the Active Disturbance Rejection Control [40], which is adopted to observe both the states of the robot system (z_1 and z_2) and the total disturbance z_3 of the robotic joint system.

Consequently, the fSMC-ESO control system for human-like motion of the joint can be described by Eqs. (17) and (18), and it is able to inhibit the disturbance and compensate the nonlinearity of the PAM system and achieve the expected tracking control performance with the control input:

$$u = -b^{-1}(-\ddot{x}_d + z_3 - c_2 \text{sign}(\dot{e})|\dot{e}|^{\alpha_2} - c_1 \text{sign}(e)|e|^{\alpha_1} + u_n) \quad (19)$$

3.4 Experimental validations

The proposed approach is validated via physical experiments on the platform of **Figure 9**. The PAMs are FESTO DMSF-20-200 with pre-tension of 40 N, and the parameters of the PAM model as well as those of the robotic joint are presented in **Tables 2** and **3**, respectively. In the physical experiments, the sampling time is

Parameter	k_{11}	k_{12}	k_{21}	k_{22}	k_{31}	k_{32}	L_0 (m)
Value	2.573	-222.7	6.389	1347.3	0.296	141.5	0.2

Table 2.
Parameters of mathematical model of PAMs.

Parameter	m_{pulley} (kg)	r (m)	m (kg)	l (m)	f_b (N s/m)
Value	0.2	0.016	3	0.2	0.2

Table 3.
 Parameters of the robotic joint.

0.01s, $x_f = 90^\circ$, $t_f = 2s$, and the force of the antagonistic muscle is constant $F_2 \equiv 40N$.

The performance of the fSMC-ESO approach against disturbance is validated via simulations of no external disturbance ($d = 0$), constant external disturbance ($d = 2rad$), and variable external disturbances (sinusoidal signal, $d = 2 \sin(2\pi t)$, and $d = 2 \sin(\pi t)$). The simulation results (both the output of the control system and the result of state observation) are presented in **Figure 11**, which validates that the ESO can accurately observe the state variation (including the external disturbances) of the system; as a result, the bionic joint is able to track the desired motion curve under different disturbances with an acceptable small error amplitudes under sinusoidal disturbances (0.006 and 0.001 of $d = 2 \sin(2\pi t)$ and $d = 2 \sin(\pi t)$, respectively).

Then, the robustness of the proposed fSMC-ESO approach to the payload variation is validated in **Figure 12**, which illustrates the tension, the pressure, and the length of the antagonistic PAMs in the course of human-like motion with payload of 1 kg, 3 kg, and 5 kg, respectively. The fSMC-ESO approach can adjust the air pressure of PAMs according to load variation; as a result, it is robust to the payload variation and at the same time keeps good performance of human-like motion.

Figure 13 illustrates the physical experiment result of the robotic joint system, which achieves the expected human-like motion with a small overshoot (less than 1.2%, i.e., 1.1 degrees of angle). An estimated initial value of the total disturbance ($z_3(0) = 130$), which can be approximately determined via simulations and accordingly adjusted in the experiment, is applied to suppress the fluctuations at the initial period of the rise time so as to improve the performance of the control system. At the time of 6.5 s, an external disturbance is exerted on the robotic arm, and the control system is able to suppress the disturbance and drive the platform back to its primary position within 1 s. The good performances of trajectory tracking and robustness of the robotic joint system are reasonably attributed to both the state observing ability of ESO and the nonlinear control ability of fSMC.

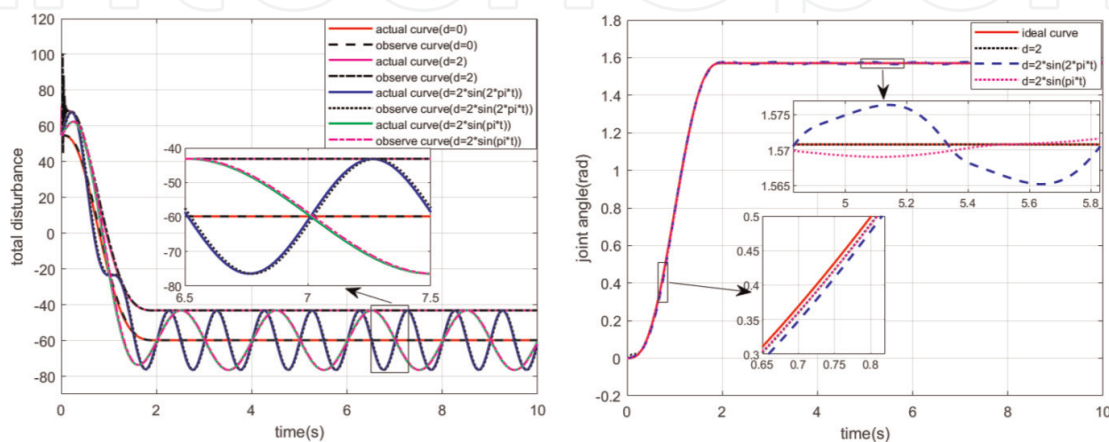


Figure 11.
 Simulation of observation result and the joint angle response under different disturbances.

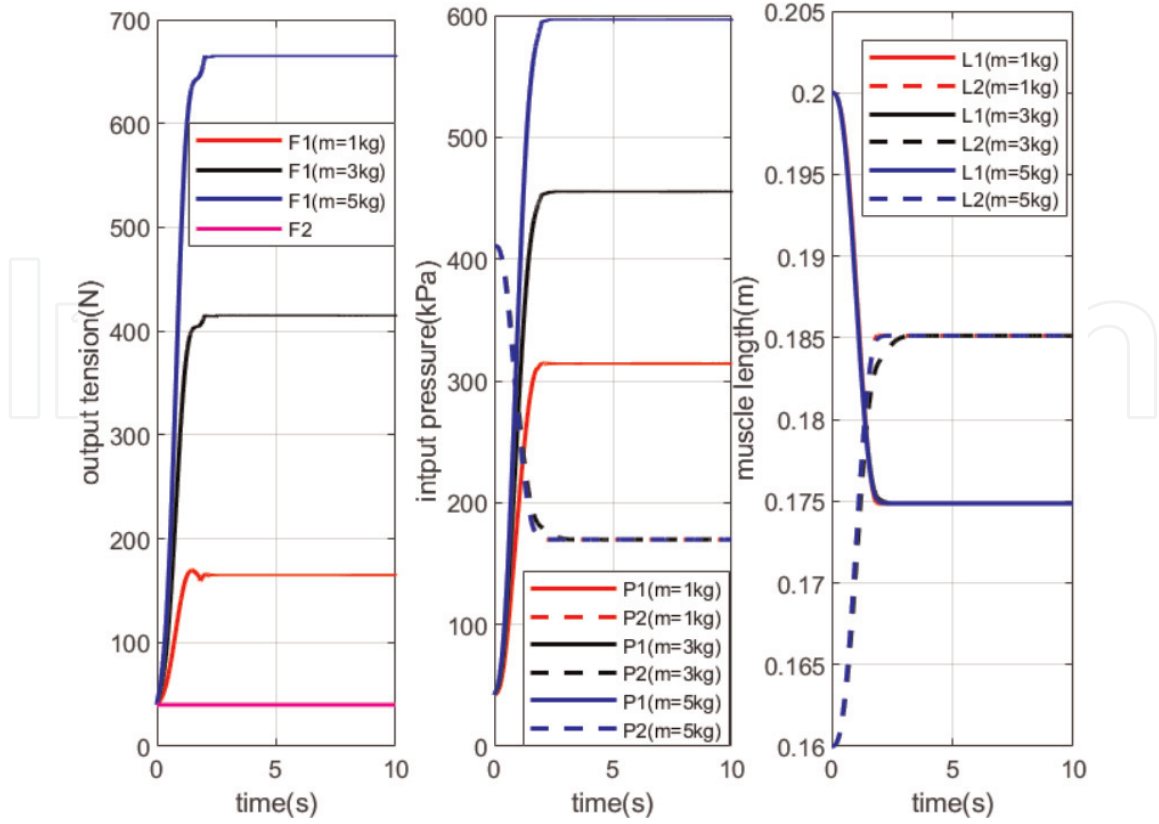


Figure 12. Simulation result of the tension, pressure, and length of the PAMs with different payloads.

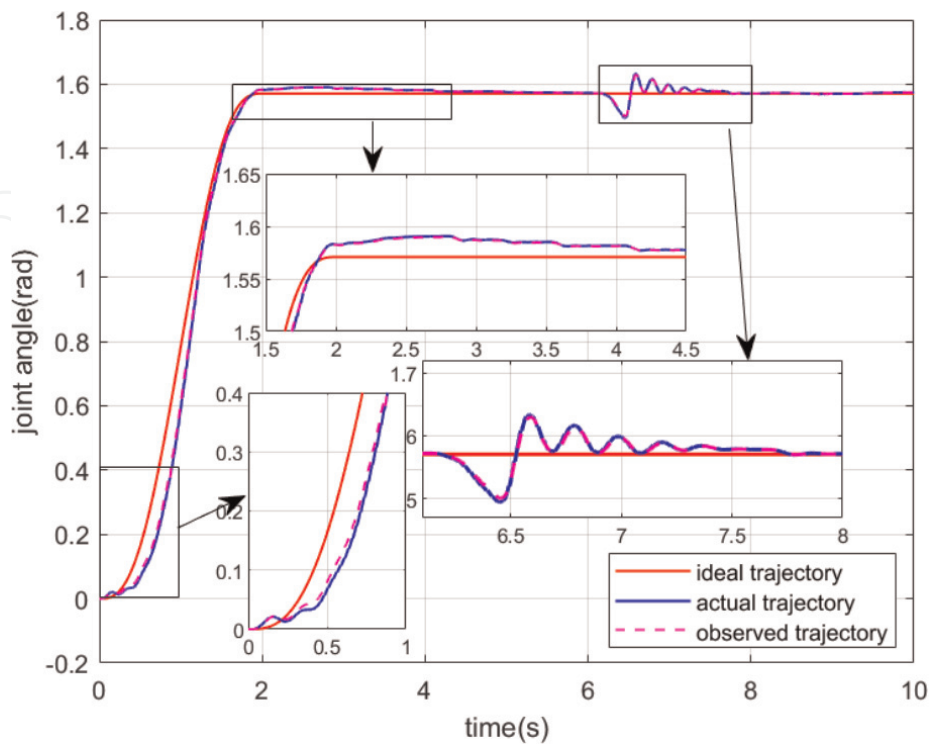


Figure 13. Physical experiment result of the angular trajectory of the robotic joint ($z_3(0) = 130$).

3.5 Summary

It is generally acknowledged that it is very difficult to model PAM precisely, and the model imprecision, which, caused by both nonlinearities (including hysteresis effects) and the uncertainty of parameters, will severely impede the control performance of the PAM system. The fSMC-ESO approach views the model imprecision as a kind of internal disturbance, observes both the external and internal disturbances via ESO, and compensates them via fSMC to realize the human-like motion with expected robustness and tracking accuracy. As validated in this experiment, though the hysteresis effects of the PAM are completely ignored by taking only one part of Yu's model (these two parts obviously different from each other) into consideration, this approach still is able to achieve good control performance of the robotic joint system. Therefore, the fSMC-ESO approach can be applied to solve the model imprecision problems of the PAM systems and consequently improve their control performance.

4. Limitations and relevant promising studies of PAM systems

PAMs do possess some distinct advantages, which are favorable for the actuation of the cooperative robots; it also has some unfavorable properties except the strong nonlinearities and the uncertainty of parameters that can be properly handled as abovementioned. These topics are briefly discussed as follows:

4.1 The pressured air source issue

PAM works with the compressed air as mediator, and via the outlet valve, it vents the high-throughput compressed air to the atmosphere. Therefore, a PAM system requires a pressured air source, e.g., an air compressor with high-pressure gas pot, which undoubtedly will make the PAM system bulky.

A solution of this issue is to make the working medium recyclable. Therefore, researchers studied the Hydraulic McKibben Artificial Muscles (HAMs), which take the hydraulic oil or water instead of pressed air as the working fluid.

The most impressive advantage of the HAMs is its supper high energy efficiency, e.g., a prototype high force HAM, which is 40 mm in diameter and 700 mm in length and driven by a maximum water hydraulic of pressure of 4 MPa, can achieve a maximum contracting force of 28 kN [41]. However, HAMs also degrade its inherent compliance because of the incompressible hydraulic working fluid. Furthermore, HAMs did not solve the bulky size problem of PAMs, because it also needs a reservoir, as well as pumps and valves to supply the pressured working fluid.

4.2 The dilemma of the output torque and the motion range of a joint

As illustrated in both the **Figure 2** and the Eq. (1), the PAMs' contraction length ε equals the arc length on the pulley circumference corresponding to the rotary scope ϑ of the joint. For a given item of PAM, the contraction length is a constant, and the pulley radius should be limited so as to cover the required joint rotation angle with the constant contraction length. Consequently, the joint torque $T = F \cdot r$ is limited, which will restrict the application of PAMs in robotic systems.

One can obtain a higher joint torque either via a higher contraction force F or via a larger pulley radius r .

The former method is known as the Variable Recruitment Strategy (VRS), which parallelly deploys many PAMs as a muscle bundle and recruits different number of PAMs according to the output torque requirement [42]. VRS recruits 1, 2, or 3 pairs of PAMs to generate different force for meeting the application requirement, respectively. Consequently, the robotic system is able to realize the expected actuating performance with the minimal activated number of PAMs for increasing the efficiency of the PAM system.

However, the VRS has some drawbacks that impede its robotic application:

1. The PAMs are parallelly deployed to generate a variable output torque via a variable number of recruitments, while both the contraction length and the pulley radius of the PAM group configuration are the same as those of a single pair of PAM configuration, the power efficiency of the joint therefore is not high;
2. In the working process, the PAMs did not be activated (still with an amount of air in it) will be bended or buckled, which will generate a certain resistance and degrade the drive performance of the joint. Furthermore, the frequent bending will seriously shorten the life span of PAMs;
3. The group of PAMs must be exactly parallelly deployed as a muscle bundle to draw the same steel wire. It consequently will make the system bulky and impede the deployment and application of the VRS PAMs group in a robotic system.

The latter method sequentially deploys and activates multiple PAMs via a large pulley to generate a high output torque. As illustrated in **Figure 14**, in order to drive the joint rotating a certain angle, multiple PAMs are activated one after the other, and the total arc length of the pulley circumference corresponding to the rotary scope of the joint is therefore assigned to the total contraction length of these PAMs rather than those of one PAM. An overrunning clutch is employed to transmit the driving torques of PAMs to the joint axis. As a result, the PAMs generate a high output torque on a larger pulley radius than those of the VRS approach.

The second approach is expected to solve the aforementioned problems of the VRS approach and accordingly show the following advantages:

1. Higher power efficiency. Because it generates the driving torque of the joint via a larger pulley radius and less energy consumption;
2. Flexible deployment of the PAMs. PAMs of a joint are no longer need to be parallelly deployed as a muscle bundle. Therefore, the volume of a joint can be

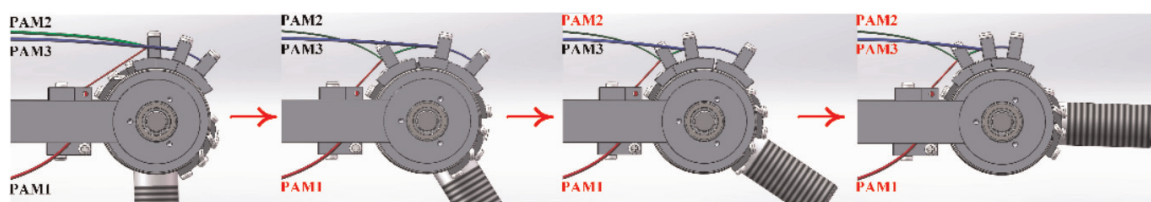


Figure 14.
The sequential activation approach (PAMs in red means be activated).

reduced for convenient of manipulations, and the PAMs will have a longer life span because they will not be bent anymore.

4.3 The flexibility and shape adaptability for soft wearable robot applications

The PAMs are considered a good actuator for wearable robot systems, i.e., the exosuit and the exoskeleton robot, because of its compliance characteristics and the human-muscle-like contraction properties. However, the PAMs commonly used are large in size (10–40 mm in diameter and 100+ mm in length) and rigid in use (drastically stiffen when inflated), which make them unsuitable to be applied to wearable robot applications. The wearable robots require the flexibility and shape adaptability of PAMs for compliantly deforming along with the human body and redundant human-muscle-like actuation mechanism.

A promising study for this problem is the thin McKibben muscle (TMM) or multifilament muscles [43]. When a group of the TMMs with an outer diameter of 1.8 mm are bundled as a robotic actuator, it is flexible (even when pressurized), compact, and lightweight to be easily attached to the complex or irregularly shaped parts of the robots for actuation. Especially, TMMs are deformable to follow the human body shape, as well as taking various shapes to mimic the human muscle shapes, e.g., the biceps, the triceps, and the flat muscles of the pectoralis major or the deltoid muscles, for realizing a human-friendly support and power assistance.

Furthermore, the structural feature of multifilament makes TMM a perfect choice for mimicking both the structure and the recruitment mechanism of the skeletal muscle. Each skeletal muscle has a finite number of motor units, which is the smallest subunit of a muscle that can be recruited and consists of a certain number of muscle fibers 100 μm in diameter. The fiber number of a motor unit varies from 3 (for the fine control of the eyes) to 2000 (for the vigorous motion of the legs) according to its location and function [44]. The human central nervous system will excite (recruit) appropriate number of motor units according the task requirement for the optimization of actuation efficiency. The aforementioned VRS of PAMs is exactly an attempt for this propose, while the multifilament structure of TMM makes it a more suitable choice for imitating the recruitment mechanism of the human skeletal muscles.

TMMs have the same limitation of PAMs, i.e., they require a pressurized fluid source supplied by an external pump or compressor, which are generally rigid and bulky, and consequently preventing untethered and portable operations.

A promising study to this issue is the pumps based on the principle of ElectroHydroDynamics. Cacucciolo et al. studied a solid-state pumping mechanism that directly accelerates the working medium of dielectric liquid by means of an electric field [45]. This pump is silent, fully stretchable, and bendable while operating, which makes it a very promising solution for the TMMs actuated soft wearable robot.

5. Conclusions

The McKibben PAMs possess some compelling properties, e.g., the inherent compliance, the actuating characteristics similar to those of the human muscle, the flexibility of deployment, etc. These properties make PAM an excellent actuator for the humanoid robot systems. Focused on the robot application of PAMs, this chapter concerned the following critical techniques:

Firstly, this chapter presented a solution for the PAM system design. People have tried hard to realize the human-like dexterous operational capability via highly biomimetic design that mimics the musculoskeletal structure of human body in the design of robot system, but inevitably lead to high complexity in structure and difficulty for manufacture and control. In order to solve this problem, this chapter in detail presented the bionic design of a 7 DOF human-arm-like manipulator. This design mimics the human arm in functionality rather than in construction. It takes the antagonized PAMs and Bowden cables that mimic the muscle-tendon-ligament structure of human body and elaborately configures the DOFs of the arm and flexibly deploys the routing of Bowden cables. As a result, the joints of the analog shoulder, elbow, and wrist of the robotic arm intersect at a point respectively though these DOFs are sequentially arranged, and the motions of these joints are independent from each other for convenience of motion control and human-like dexterous manipulation. If motors instead of PAMs are taken as the actuators of the robotic arm, it will be very difficult to make the joints of the analog shoulder, elbow, and wrist intersect at a point respectively, and the robotic arm will be offset and bulky because of the volume of the motors and reduction gears.

Secondly, this chapter presented a solution for the tracking motion control of the PAM system. It is universally acknowledged that the PAM is very difficult for modeling and control because of its strong nonlinear characteristics. This chapter proposed a fSMC-ESO approach to realize the human-like motion control of the robotic joint. This approach views the model imprecision caused by the strong nonlinearity of the PAMs as a kind of internal disturbance of the robotic system and combines ESO with fSMC to observe and compensate the external and internal disturbances. Experiments validated that the fSMC-ESO approach is able to realize the human-like motion with expected robustness and tracking accuracy, though the model of PAM is obviously inaccurate because only one part of the Yu's model is taken into consideration. Therefore, it can be concluded that the fSMC-ESO approach has remarkable advantages for solving the model imprecision problems and achieving good control performance for the PAM systems.

Thirdly, some variants of PAMs that are aiming to amend or remedy the drawbacks of the PAM systems are discussed. Especially, a Sequential Activation approach that targets to the dilemma of the output torque and the motion range of a PAM actuated joint is proposed. Different from the others, this approach sequentially deploys and activates multiple PAMs via a large pulley and an overrunning clutch to generate a high output torque at the same time cover the total rotary scope of the joint, and it may also bring advantages of higher power efficiency and more flexible deployment of the PAM systems.

As a conclusion, the McKibben PAM actuator is a promising solution for the advanced robotic systems, and the PAM-based inherent safety and compliant manipulation will certainly play an important role in the cooperative humanoid robots. With further research, people can optimistically anticipate the wide applications of the PAM actuated robotic systems in the human living environment.

Acknowledgements

This work was supported by the National Natural Science Foundation of China (grant number: 61673003) and the Natural Science Foundation of Beijing Municipality (grant number: 4192010).

Conflict of interest

The authors declare no conflict of interest.

IntechOpen


IntechOpen

Author details

Daoxiong Gong* and Jianjun Yu
Faculty of Information Technology, Beijing University of Technology, Beijing, China

*Address all correspondence to: gongdx@bjut.edu.cn

IntechOpen

© 2022 The Author(s). Licensee IntechOpen. This chapter is distributed under the terms of the Creative Commons Attribution License (<http://creativecommons.org/licenses/by/3.0>), which permits unrestricted use, distribution, and reproduction in any medium, provided the original work is properly cited. 

References

- [1] Ding H, Yang X, Zheng N, et al. Tri-Co Robot: A Chinese robotic research initiative for enhanced robot interaction capabilities. *National Science Review*. 2017;5:799-801. DOI: 10.1093/nsr/nwx148
- [2] Daerden F, Lefeber D. Pneumatic artificial muscles: Actuators for robotics and automation. *European Journal of Mechanical and Environmental Engineering*. 2002;47(1):10-21
- [3] Andrikopoulos G, Nikolakopoulos G, Manesis S. A survey on applications of pneumatic artificial muscles. In: *The 19th Mediterranean Conference on Control and Automation*; 20-23 June 2011; Greece. New York: IEEE; 2011. pp. 1439-1446
- [4] Klute K, Czerniecki J, Hannaford B. Artificial muscles: Actuators for biorobotic systems. *The International Journal of Robotics Research*. 2002; 21(4):295-309
- [5] Airic's arm—Festo [Internet]. Available from: https://www.festo.com/net/SupportPortal/Files/42058/Airics_arm_en.pdf [Accessed: November 01, 2021]
- [6] Robotic Hands That Mimic Human Movement with Air Muscles [Internet]. Available from: <https://www.techeblog.com/feature-robotic-hands-that-mimic-human-movement-with-air-muscles/> [Accessed: November 01, 2021]
- [7] Nanayakkara V, Cotugno G, Vitzilaios V, et al. The role of morphology of the thumb in anthropomorphic grasping: A review. *Frontiers in Mechanical Engineering*. 2017;3(5):1-21. DOI: 10.3389/fmech.2017.00005
- [8] Xu Z, Todorov E. Design of a highly biomimetic anthropomorphic robotic hand towards artificial limb regeneration. In: *The 2016 IEEE International Conference on Robotics and Automation (ICRA)*; 16-21 May 2016; Stockholm. New York: IEEE; 2016. pp. 3485-3492
- [9] Faudzi A, Ooga J, Goto T, et al. Index finger of a human-like robotic hand using thin soft muscles. *IEEE Robotic and Automation Letters*. 2018;3(1):92-99
- [10] Tasi B, Koller M, Cserey G. Design of the anatomically correct. *Biomechatronic the Hand*. 2019. Available from: <https://arxiv.org/ftp/arxiv/papers/1909/1909.07966.pdf> [Accessed: 2021-12-01]. DOI: arXiv: 1909.07966
- [11] Ikemoto S, Kannou F, Hosoda K. Humanlike shoulder complex for musculoskeletal robot arms. In: *2012 IEEE/RSJ International Conference on Intelligent Robots and Systems*; 7-12 October 2012; Vilamoura. New York: IEEE; 2012. pp. 4892-4897
- [12] Andrikopoulos G, Nikolakopoulos G. Design, development and control of a human-inspired two-arm robot via pneumatic artificial muscles. In: *2017 25th Mediterranean Conference on Control and Automation (MED)*; July 2017; Valletta. New York: IEEE; 2017. pp. 241-246
- [13] Andrikopoulos G, Nikolakopoulos G, Kominiak D, Unander-Scharin A. Towards the development of a novel upper-body pneumatic humanoid: Design and implementation. *2016 European Control Conference (ECC)*; 2016; Aalborg. New York: IEEE; 2016. pp. 395-400

- [14] Lilly J, Liang Y. Sliding mode tracking for pneumatic muscle actuators in opposing pair configuration. *IEEE Transactions on Control Systems Technology*. 2005;**13**:550-558
- [15] Estrada A, Plestan F. Second order sliding mode output feedback control with switching gains—Application to the control of a pneumatic actuator. *Journal of the Franklin Institute*. 2014;**351**: 2335-2355
- [16] Shi G, Shen W. Hybrid control of a parallel platform based on pneumatic artificial muscles combining sliding mode controller and adaptive fuzzy CMAC. *Control Engineering Practice*. 2013;**21**:76-86
- [17] Amar R, Tondu B, Hamerlain M. Experimental study of nonsingular terminal sliding mode controller for robot arm actuated by pneumatic artificial muscles. *IFAC Proceedings*. 2014;**47**:10113-10118
- [18] Rezoug A, Boudoua S, Hamerlain F. Fuzzy logic control for manipulator robot actuated by pneumatic artificial muscles. *Journal of Electrical Systems*. 2009;**9**:1-6
- [19] Büchler D, Calandra R, Schölkopf B, Peters J. Control of musculoskeletal systems using learned dynamics models. *IEEE Robotics and Automation Letters*. 2018;**3**:3161-3168
- [20] Song C, Xie S, Zhou Z, Hu Y. Modeling of pneumatic artificial muscle using a hybrid artificial neural network approach. *Mechatronics*. 2015;**31**:124-131
- [21] Ahn K, Nguyen H. Intelligent switching control of a pneumatic muscle robot arm using learning vector quantization neural network. *Mechatronics*. 2007;**17**:255-262
- [22] Chang M, Liou J, Chen M. T-S fuzzy model-based tracking control of a one-dimensional manipulator actuated by pneumatic artificial muscles. *Control Engineering Practice*. 2011;**19**:1442-1449
- [23] Chandrapal M, Chen X, Wang W, Hann C. Nonparametric control algorithms for a pneumatic artificial muscle. *Expert Systems with Applications*. 2012;**39**:8636-8644
- [24] Sadrfaridpour B, Wang Y. Collaborative assembly in hybrid manufacturing cells: An integrated framework for human-robot interaction. *IEEE Transactions on Automation Science and Engineering*. 2017;**15**: 1178-1192
- [25] Bortot D, Born M, Bengler K. Directly or on detours? how should industrial robots approximate humans? In: *The 8th ACM/IEEE International Conference on Human-Robot Interaction*; 3–6 March 2013; Tokyo. New York: IEEE; 2013. pp. 89-90
- [26] Kato R, Fujita M, Arai T. Development of advanced cellular manufacturing system with human-robot collaboration. In: *The 19th International Symposium in Robot and Human Interactive Communication*; 13-15 September 2010; Viareggio. New York: IEEE; 2010. pp. 355-360
- [27] Zanchettin A, Bascetta L, Rocco P. Achieving humanlike motion: Resolving redundancy for anthropomorphic industrial manipulators. *IEEE Robotics & Automation Magazine*. 2013;**20**: 131-138
- [28] Kulic D, Venture G, Yamane K, et al. Anthropomorphic movement analysis and synthesis: A survey of methods and applications. *IEEE Transactions on Robotics*. 2016;**32**(4):776-795

- [29] Berret B, Jean F. Why don't we move slower? The value of time in the neural control of action. *The Journal of Neuroscience*. 2016;**36**:1056-1070
- [30] Terlemez Ö, Ulbrich S, Mandery C, et al. Master Motor Map (MMM)—Framework and toolkit for capturing, representing, and reproducing human motion on humanoid robots. In: 2014 IEEE-RAS International Conference on Humanoid Robots; Madrid. New York: IEEE; 2014. pp. 894-901
- [31] Gong D, He R, Wang Y, Yu J. Bionic design of a 7-DOF human-arm-like manipulator actuated by antagonized pneumatic artificial muscles. In: The 9th IEEE International Conference on CYBER Technology in Automation, Control, and Intelligent Systems; 29 July 29—2 August 2019; Suzhou. New York: IEEE; 2020. pp. 1503-1508
- [32] Gong D, Hao L, Yu J, Zuo G. Bionic design of a dexterous anthropomorphic hand actuated by antagonistic PAMs. In: The 2020 IEEE International Conference on Real-time Computing and Robotics; 28-29 September 2020. Asahikawa. New York: IEEE; 2020. pp. 493-498
- [33] Gong D, He R, Yu J, et al. A pneumatic tactile sensor for co-operative robots. *Sensors*. 2017;**17**:2592. DOI: 10.3390/s17112592
- [34] Dahiya RS, Metta G, Valle M, et al. Tactile sensing-From humans to humanoids. *IEEE Transactions on Robotics*. 2010;**26**(1):1-20. DOI: 10.1109/TRO.2009.2033627
- [35] Gong D, Pei M, He R, Yu J. An extended state observer-based full-order sliding mode control for robotic joint actuated by antagonistic pneumatic artificial muscles. *International Journal of Advanced Robotic Systems*. 2021;1-11. DOI: 10.1177/1729881420986036
- [36] Flash T, Hogan N. The coordination of arm movements: An experimentally confirmed mathematical model. *The Journal of Neuroscience*. 1985;**5**:1688-1703
- [37] Yu H, Guo W, Tan H, et al. Design and control on antagonistic bionic joint driven by pneumatic muscles actuators. *Journal of Mechanical Engineering*. 2012;**48**:1-9 (in Chinese). DOI: 10.3901/JME.2012.17.001
- [38] Feng Y, Han F, Yu X. Chattering free full-order sliding mode control. *Automatica*. 2014;**50**:1310-1314
- [39] Gao Z. Scaling and bandwidth-parameterization based controller tuning. In: The 2003 American control conference; 4-6 June 2003; Denver. New York: IEEE. 2003;**6**:4989-4996
- [40] Huang Y, Xue W. Active disturbance rejection control: Methodology and theoretical analysis. *ISA Transactions*. 2014;**53**:963-976
- [41] Mori M, Suzumori K, Takahashi M, et al. Very high force hydraulic McKibben artificial muscle with a p-phenylene-2, 6-benzobisoxazole cord sleeve. *Advanced Robotics*. 2010;**24**: 233-254
- [42] Meller M, Chipka J, Volkov A, et al. Improving actuation efficiency through variable recruitment hydraulic McKibben muscles: Modeling, orderly recruitment control, and experiments. *Bioinspiration & Biomimetics*. 2016;**11**: 065004. DOI: 10.1088/1748-3190/11/6/065004
- [43] Kurumaya S, Nabae H, Endo G, et al. Design of thin McKibben muscle and

multifilament structure. *Sensors and Actuators A*. 2017;**261**:66-74

[44] Winter DA. *Biomechanics and Motor Control of Human Movement*. 4th ed. Hoboken: John Wiley & Sons; 2009.
DOI: 10.1002/9780470549148

[45] Cacucciolo V, Shintake J, Kuwajima Y, et al. Stretchable pumps for soft machines. *Nature*. 2019;**572**:516-519.
DOI: 10.1038/s41586-019-1479-6

IntechOpen